Thermal changes of the crystal structure and the influence of thermo-chemical annealing on the optical properties of $YbAlO_3$ crystals

2010 J. Phys.: Condens. Matter 22 055902

(http://iopscience.iop.org/0953-8984/22/5/055902)

J. Phys.: Condens. Matter **22** (2010) 055902 (7pp) doi:10.1088/0953-8984/22/5/055902

Thermal changes of the crystal structure and the influence of thermo-chemical annealing on the optical properties of $YbAlO_3$ crystals

O Buryy[1], Ya Zhydachevskii[1], L Vasylechko[1], D Sugak[2], N Martynyuk[1], S Ubizskii[1] and K D Becker[3]

[1] Lviv Polytechnic National University, Bandery Street 12, 79013 Lviv, Ukraine
[2] R&D Institute for Materials, Scientific Research Company 'Carat', Stryjska Street 202, 79031 Lviv, Ukraine
[3] Institute of Physical and Theoretical Chemistry, Braunschweig University of Technology, Hans-Sommer straße 10, D-38106 Braunschweig, Germany

E-mail: crystal@polynet.lviv.ua

Received 12 August 2009, in final form 30 November 2009
Published 19 January 2010
Online at stacks.iop.org/JPhysCM/22/055902

Abstract
The paper presents experimental results of investigations on the influence of temperature and thermo-chemical annealing on the structural and optical properties of $YbAlO_3$ crystals. Thermal behaviour of the crystal structure has been studied in the temperature range of 19–1173 K by means of *in situ* high-resolution x-ray powder diffraction using synchrotron radiation. Lattice expansion of $YbAlO_3$ displays a strongly anisotropic character: the relative expansion along the *b* direction is about two times smaller than that along the *a* and *c* axes. The influence of thermo-chemical annealing in oxidizing and reducing atmospheres has been studied by means of *in situ* optical spectroscopy. The increase of the absorption in the range of 300–600 nm during annealing in an oxidizing atmosphere as well as its bleaching during reduction has been observed in the temperature range 700–1000 K. The oxidation and reduction kinetics have been analysed by means of mathematical models taking into account diffusion and the quasi-chemical reaction of the defect centres.

1. Introduction

Recently, ytterbium aluminium perovskite (ytterbium orthoaluminate) single crystals, $YbAlO_3$ (YbAP), have attracted considerable attention because of their potential application as materials for effective and fast scintillators. In particular, $YbAlO_3$ crystals are considered for prospective use for radiation detectors [1], especially for solar neutrinos (ν_e) [2]. In addition, single crystals of $YbAlO_3$, as well as of yttrium aluminium perovskite $YAlO_3$ (YAP), doped with manganese can be used for effective optical data storage [3]. All these applications need crystals of high optical quality, in particular with insignificant absorption in the visible and UV spectral range. However, the as-grown $YbAlO_3$ crystals exhibit a noticeable absorption in this part of the spectrum which, however, can be removed by after-growth annealing in reducing atmospheres or in vacuum.

The present work is devoted to *in situ* investigations of the influence of temperature and thermo-chemical treatment on the structural and optical properties of $YbAlO_3$ single crystals. It aims at a better understanding of the processes taking place in this complex oxide crystal under the influence of elevated temperatures and appropriate gas environments.

2. Experimental details

The method of obtaining $YbAlO_3$ single crystals studied in the present work is described in [3]. The crystal was grown by the Czochralski technique in an iridium crucible in a nitrogen atmosphere with 0.2% oxygen. The ytterbium orthoaluminate

was nucleated on iridium wires. It became single crystalline after several millimetres of pulling, and the final orientation of the boule was close to the crystallographic *c* axis. The pull rate is 1.5 mm h^{-1} and the rotation rate is 15 rpm [3].

The crystal structure of $YbAlO_3$ and its thermal behaviour over a wide temperature range of 20–1173 K have been studied in detail by means of x-ray single-crystal and powder diffraction techniques using synchrotron radiation. Both single-crystal and powder diffraction experiments have been carried out at the synchrotron facility HASYLAB/DESY. For structural determination, a twin-free single-domain plate-like shaped crystal was selected from a single-crystal boule after careful examination.

The room temperature single-crystal diffraction experiment was performed at the Kappa-diffractometer of beamline F1 equipped with a SMART CCD system. Data collection was performed at the wavelength of 0.565 Å under the following experimental conditions: crystal-detector distance 40.0 mm, omega scan mode ($\Delta\omega = 0.1°$, $t = 2$–10 s) and SAINT parameters (xy/z integration box size): 2.0°/0.12°. A set of 3060 reflections were collected at eight different φ settings covering 91° in omega, ensuring a coverage of ∼100% (in *mmm* symmetry). The typical FWHM of the reflections was 0.05°. The lattice parameters were calculated using the orientation matrices incorporating correction factors (diffractometer zeros, CCD camera miss setting, etc). The integration was performed with SAINT using an integration box size of $xy/z = 2.0°/0.12°$. A correction for systematic errors, absorption and scaling was done using SADABS by fitting spherical harmonic functions following the method of Blessing [4].

The *in situ* low- and high-temperature diffraction experiments were performed at beamline B2 of the powder diffractometer equipped with an on-site readable image plate detector OBI, a closed-cycle cryostat and an STOE furnace [5–7]. The polycrystalline (powdered) sample used for the investigation was prepared from the same single-crystal ingot which had been used for further optical investigations.

Data analysis and all crystallographic calculations were performed within the WinCSD program package [8]. Details of the synchrotron diffraction experiments, the data evaluation and some preliminary results can be found in [9–11].

The optical *in situ* experiments have been performed using a specially designed high-temperature furnace placed in a Perkin-Elmer Lambda 900 spectrophotometer, see [12, 13] for details. Absorption spectra of a $YbAlO_3$ crystal were measured in the range from 290 to 1200 nm at temperatures up to 1013 K. The experimental quantity determined in the experiments is an absorbance $A = \lg(I_0/I)$, where I and I_0 represent the intensities of transmitted and incoming light, respectively. Samples for optical investigations were prepared as non-oriented flat-parallel plates with polished surfaces and sizes of about $5 \times 5 \times 0.9$ mm^3. The gas supply system with controlled flow provides a well-defined atmosphere in the furnace. The main feature of the set-up used is the possibility of rapid (∼1 min) replacement of gas atmospheres in the furnace and the registration of the subsequent reduction/oxidation kinetics at a certain wavelength. Pure oxygen was used as an oxidizing atmosphere and a mixture of gases $95\%Ar + 5\%H_2$ was used as the reducing one. The kinetics of absorbance changes were registered at a wavelength of 450 nm, which roughly corresponds to the maximum of the absorption band formed during oxidation. At elevated temperatures (>750 K), heat radiation emitted from the furnace and the sample makes a significant contribution to the intensity of light measured by the spectrophotometer. In this case the measured intensity I_m is equal to the sum $I+I_r$, where I, as previously, is the intensity of transmitted light and I_r is the intensity of heat radiation. To avoid the contribution of heat radiation, the absorption spectra measured at elevated temperatures were corrected as follows. Beside the measured value of the absorbance $A_m = \lg(\frac{I_0}{I_m}) = \lg(\frac{I_0}{I+I_r})$, the value $A_r = \lg(\frac{I_0}{I_r})$ was measured when the incoming light was blocked by a screen. The absorbance of the sample A was derived from the measured intensities A_m and A_r as

$$A = \lg\left(\frac{I_0}{I}\right) = -\lg\left(10^{-A_m} - \frac{I_r}{I_0}\right) = -\lg(10^{-A_m} - 10^{-A_r}). \quad (1)$$

To take into account the reflection of light at the surfaces of the sample, the term $-2\lg(1-R)$ should be added to the right-hand part of (1). It leads to an increase of the absorbance A by about 0.1 in the whole spectral region investigated and, thus, causes no additional structure in the spectrum. The same result was previously obtained for $LiNbO_3$:MgO single crystals [14].

3. Experimental results

3.1. Crystal structure

According to the x-ray synchrotron single-crystal diffraction study, at room temperature, $YbAlO_3$ possess the distorted orthorhombic $GdFeO_3$ type of crystal structure (space group *Pbnm*, $a = 5.1261(1)$ Å, $b = 5.3314(1)$ Å, $c = 7.3132(2)$ Å). Full-matrix least-squares refinement of the structure with anisotropic approximation of displacement parameters for all atoms, performed in space group *Pbnm* by using 604 averaged reflections with $F > 4\sigma(F)$, resulted in reliability factors of $R_F = 0.058$ and $R_W = 0.042$. Final results of the structural refinement of $YbAlO_3$ are summarized in table 1.

The *in situ* powder diffraction experiments applying synchrotron radiation as well as neutrons revealed no structural changes in a broad temperature range of 4.2–1173 K [10, 11, 15]. Refined structural parameters of $YbAlO_3$ including cell dimensions, positional and displacement parameters of atoms at selected temperatures of 4.2, 100, 298 and 1173 K are summarized in [16]. The thermal expansion of ytterbium orthoaluminate displays an anisotropic and nonlinear behaviour. Lattice parameters a, b and c of $YbAlO_3$ are found to change with temperature as follows: $a = 5.1221(3)[1 + 1.4(2) \times 10^{-8}T^2 - 8.0(5) \times 10^{-11}T^3 + 2.1(5) \times 10^{-14}T^4]$; $b = 5.3727(3)[1 + 4.3(3) \times 10^{-9}T^2 + 1.9(4) \times 10^{-12}T^3 - 2.0(6) \times 10^{-15}T^4]$; $c = 7.301\,08(4)[1 + 3.0(2) \times 10^{-8}T^2 - 3.5(4) \times 10^{-11}T^3 + 1.4(2) \times 10^{-14}T^4]$. Figure 1 shows a relative expansion of $YbAlO_3$ in different crystallographic directions.

Table 1. Positional and displacement parameters of atoms in $YbAlO_3$ at ambient temperature.

Atom, sites	x	y	z	$B^{a}_{iso/eq}$ (Å^2)
Yb, 4c	−0.01362(6)	0.06007(5)	$\frac{1}{4}$	0.40(1)
Al, 4b	$\frac{1}{2}$	0	0	0.40(6)
O1, 4c	0.0912(11)	0.4716(8)	$\frac{1}{4}$	0.53(8)
O2, 8d	−0.3004(7)	0.2991(5)	0.0475(5)	0.55(6)

Anisotropic displacement parameters of atoms

	B_{11}	B_{22}	B_{33}	B_{12}	B_{13}	B_{23}
Yb, 4c	0.48(2)	0.48(2)	0.23(2)	−0.027(4)	0	0
Al, 4b	0.42(7)	0.45(9)	0.33(12)	0.01(4)	−0.01(4)	−0.05(11)
O1, 4c	0.61(15)	0.73(11)	0.2(2)	0.10(11)	0	0
O2, 8d	0.53(9)	0.65(8)	0.46(12)	−0.06(7)	0.04(9)	−0.08(8)

[a] $B_{iso/eq} = 1/3[B_{11}\ (a^*)^2a^2 + \cdots 2B_{23}b^*c^*bc\cos a]$;
$T = \exp[-1/4(B_{11}(a^*)^2h^2 + \cdots 2B_{23}b^*c^*kl)]$.

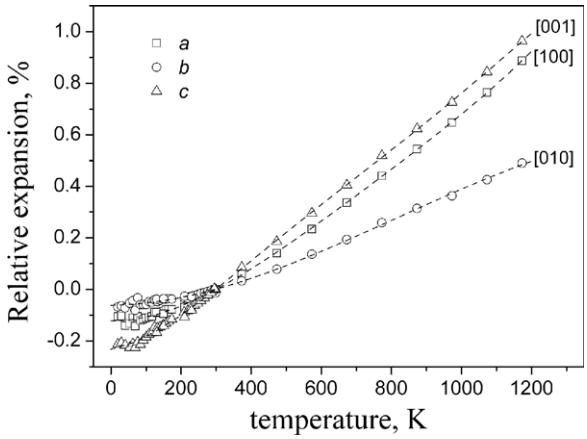

Figure 1. Relative expansion of $YbAlO_3$ calculated as: $\eta_L = \frac{L(T)-L(298)}{L(298)}100\%$, where $L(T)$ is the cell dimension at the corresponding temperature T. The dashed lines are guides for the eyes.

Similar to other $RAlO_3$ compounds with the $GdFeO_3$ type of structure [16], relative high-temperature expansion of $YbAlO_3$ in the *a* and *c* directions is similar and lies in the limits of 0.87–1% at 1200 K, whereas the thermal expansion in the *b* direction is about two times smaller. However, in contrast to the majority of $RAlO_3$ perovskites (R = Eu, Gd, Tb, Dy, Er, Tm and Y), for which pronounced anomalies in lattice expansion were observed below room temperature [16], $YbAlO_3$ expands rather 'normally' in the whole investigated temperature range of 19–1173 K.

3.2. Optical properties

A series of optical absorption spectra of $YbAlO_3$ recorded *in situ* during oxidation and reduction at 863 K is shown in figure 2. The strong absorption band near 1000 nm, observed in both the reduced and oxidized crystal, is caused by the absorption of Yb^{3+} ions (the transition $^2F_{7/2} \rightarrow {}^2F_{5/2}$) [17, 18]. It must be mentioned, that high-temperature annealing of $YbAlO_3$ crystals at temperatures up to 1013 K does not lead to a valency change of the

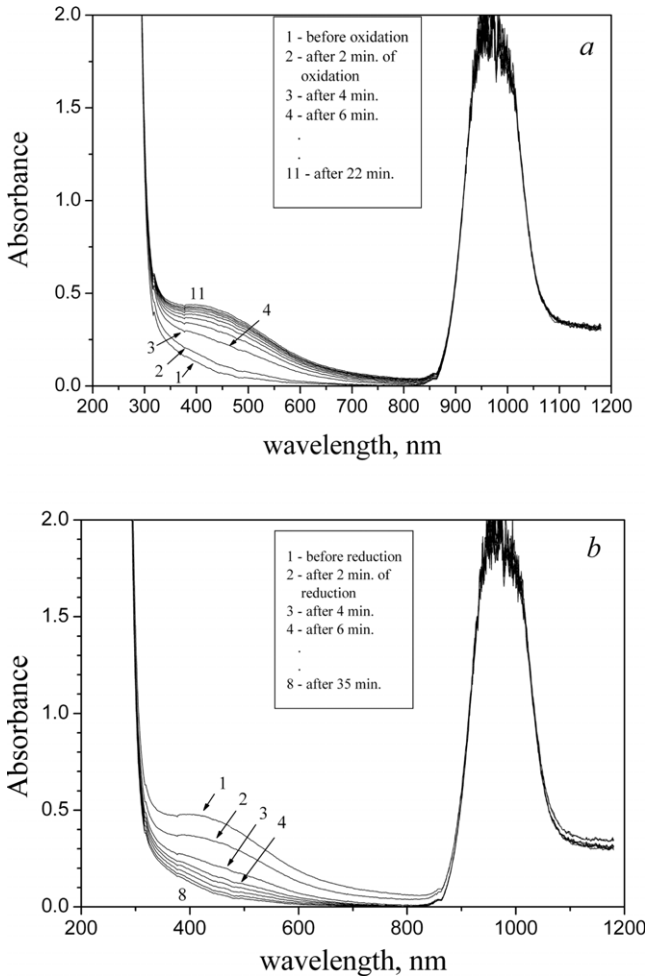

Figure 2. Changes of the absorption spectrum of $YbAlO_3$ crystal in the processes of oxidation (*a*) and reduction (*b*) at $T = 863$ K.

ytterbium(III) ions. This is in contrast to the behaviour observed for $Yb_3Al_5O_{12}$ single crystals [19] and $Yb:Y_3Al_5O_{12}$ epitaxial films [20], where changes in the optical absorption caused by the $Yb^{3+} \leftrightarrow Yb^{2+}$ recharging were observed in this spectral region. According to [21], the strong absorption of

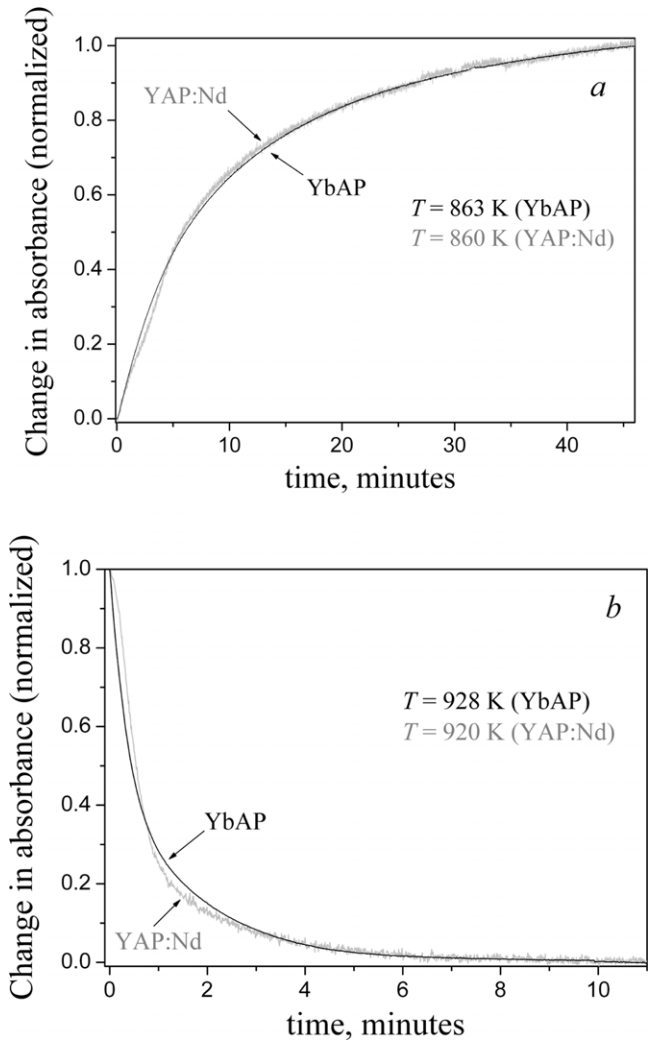

Figure 3. The comparison between the normalized kinetics of oxidation (*a*) and reduction (*b*) of YAP and YbAP single crystals registered at similar temperatures at 450 nm.

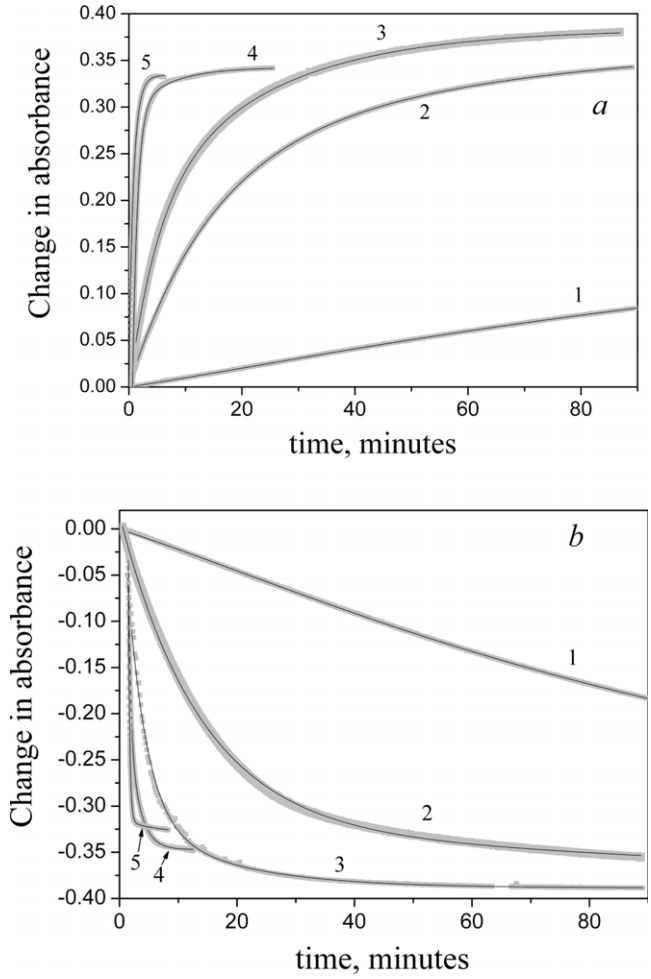

Figure 4. The kinetics of absorption changes registered at 450 nm for a YbAP single crystal during oxidation (*a*) and reduction (*b*) at 688 K (1), 773 K (2), 863 K (3), 928 K (4) and 1013 K (5) (grey lines) and their fitting in the framework of a two-component diffusion model (black lines).

$YbAlO_3$ at wavelengths below 300 nm may be caused by the charge transfer transition from the $^2F_{7/2}$ level of the Yb^{3+} ions.

The broad absorption band in the visible region (300–600 nm) is formed during oxidation. The subsequent reduction leads to bleaching of the crystal in this region. This band, obviously, is analogous to the one typical for yttrium aluminium perovskite $YAlO_3$ (YAP), which can be attributed to growth defects in the anion sublattice, namely O^- hole centres localized near anti-site yttrium ions Y_{Al} [13]. The identical nature of the bands in YAP and YbAP is also supported by the similarity of the experimental kinetics obtained for these crystals during redox processes at similar temperatures at the same wavelength of 450 nm (figure 3).

The kinetics of the absorbance changes registered at different temperatures during oxidation and reduction of $YbAlO_3$ are shown in figure 4. Note that error bars of measured absorbance are too small to show here. As seen from the figure, the temporal evolution of absorbance changes is monotonic and the durations of the oxidation and reduction processes are quite similar. They amount to minutes at temperatures above 900 K and to tens of minutes in the range 770 K $< T <$ 900 K. At temperatures around 700 K and lower, the processes taking place in $YbAlO_3$ crystals during annealing become significantly slower (curve 1 in figures 4(*a*) and (*b*)).

4. Modelling of redox kinetics of $YbAlO_3$ single crystals

Analysis of the redox processes in the $YbAlO_3$ crystal is based on models that have previously been used for describing the redox kinetics observed for YAP single crystals [13]. The main factor causing the formation/removal of absorption centres in $YbAlO_3$ is, obviously, in-diffusion of oxygen into the crystal during oxidation and its out-diffusion from the crystal during reduction. At that, any structural changes caused by the elevated temperature are not observed, as was shown above. The incorporation of oxygen into the crystal volume is dominated by diffusion of oxygen vacancies as indicated by a computer modelling of defects and transport properties in oxide perovskites [22]. A high and approximately equal quality

of fit of experimental kinetics can be achieved for $YbAlO_3$ (as well as for YAP) in the framework of the two models described below.

4.1. Diffusion model

The first model is based on the assumption that the rate of formation/disappearance of the absorption centres is directly proportional to the rate of change of the (increasing/decreasing) diffusant concentration during the redox processes. It must be mentioned that the sufficiently high precision of the approximation reached by the diffusion model is achieved only under the assumption that two different diffusion processes take place during annealing. Whereas one of them can be identified as anion vacancy diffusion, the nature of the second one cannot be determined unambiguously. Based on results for $YAlO_3$:Nd crystals [13], it can be asserted, however, that this second process is not related to proton diffusion. On the other hand, the formation and migration of oxygen interstitials have been calculated for a series of perovskites to be highly unfavourable [22]. Thus, the possibility of oxygen interstitial diffusion will be excluded also in the present case. Possibly this second process may be related to diffusion of cation vacancies formed at the crystal surface during oxidation. Somehow or other, the phenomenological character of the diffusion model neither allows nor needs to specify the atomic diffusion mechanisms responsible for the formation/disappearance of absorption centres during high-temperature annealing. Because of this ambiguity of the diffusion mechanisms involved, hereinafter we use the terms 'fast' and 'slow' for them.

The rate of change of the concentration of the absorption centres caused by the two simultaneous diffusion processes can be written as

$$\frac{\partial n_\mathrm{a}}{\partial t} = -\alpha_\mathrm{f}\frac{\partial n_\mathrm{f}}{\partial t} - \alpha_\mathrm{s}\frac{\partial n_\mathrm{s}}{\partial t}, \tag{2}$$

where n_f and n_s are the concentrations of diffusants incorporated into the crystal by the fast and slow mechanisms, correspondingly, and α_f and α_s are the respective constants of proportionality. Under the assumption of mutual independence of the fast and the slow diffusion processes, the changes of the diffusant concentration for each of them can be determined from the second Fick law [23]:

$$\frac{\partial n}{\partial t} = D\frac{\partial^2 n}{\partial^2 x}, \tag{3}$$

where $n \equiv n_\mathrm{f}$ or n_s, and D is the diffusion coefficient. For simplicity the initial distribution of the diffusant in the crystal is considered as uniform, i.e. the initial condition for equation (3) is $n(t = 0, x) = N_0$, where N_0 is a constant.

The boundary conditions for equation (3) correspond to the fact that the flux of the diffusant is continuous at the crystal surface. In accordance with the terminology of [23], they are third-order boundary conditions:

$$\begin{aligned} D\frac{\partial n}{\partial x}\bigg|_{x=0} &= R(n|_{x=0} - N_\infty), \\ -D\frac{\partial n}{\partial x}\bigg|_{x=d} &= R(n|_{x=d} - N_\infty). \end{aligned} \tag{4}$$

Here d is the crystal thickness, R is the mass-transfer coefficient and N_∞ is the concentration of diffusant at equilibrium between the crystal and surrounding gas.

The changes in the concentration of the absorption centres during annealing lead to changes of the absorbance which are calculated as

$$\Delta A(t) = \frac{\sigma}{\ln 10}\int_0^d n_\mathrm{a}(t, x)\,\mathrm{d}x - A_0, \tag{5}$$

where A_0 is the initial absorbance of the crystal and σ is the absorption cross section. Based on the solutions of equation (3) [23] and taking into account equation (2), the following expression can be obtained for the absorbance changes during annealing:

$$\begin{aligned} \Delta A(t) = \pm\Bigg(&\Delta A_{\mathrm{f}\infty}\sum_{k=0}^{\infty}\frac{8h_\mathrm{f}^2}{d(h_\mathrm{f}^2 + \lambda_{fk}^2) + 2h_\mathrm{f}}\frac{1}{\lambda_{fk}^2} \\ &\times \exp(-D_\mathrm{f}\lambda_{fk}^2 t) + \Delta A_{\mathrm{s}\infty}\sum_{k=0}^{\infty}\frac{8h_\mathrm{s}^2}{d(h_\mathrm{s}^2 + \lambda_{sk}^2) + 2h_\mathrm{s}} \\ &\times \frac{1}{\lambda_{sk}^2}\exp(-D_\mathrm{s}\lambda_{sk}^2 t)\Bigg). \end{aligned} \tag{6}$$

Here, indexes 'f' and 's' relate to the fast and the slow mechanisms correspondingly, $\Delta A_{\mathrm{f,s}\infty}$ is the maximum change of the absorbance that can be achieved due to fast/slow diffusion, the sign '+' corresponds to an increasing absorbance during annealing, i.e. to the oxidation of the $YbAlO_3$ crystal, whereas the sign '–'corresponds to its reduction, and $h_\mathrm{f,s} = R_\mathrm{f,s}/D_\mathrm{f,s}$, $\lambda_{\mathrm{f},sk}$ are the characteristic values of the Sturm–Liouville problem determined by

$$\mathrm{tg}(\lambda_{\mathrm{f},sk}d) = \frac{2h\lambda_{\mathrm{f},sk}}{\lambda_{\mathrm{f},sk}^2 + h_\mathrm{f,s}^2}. \tag{7}$$

By using equation (6) for the fitting of the experimental kinetics, the fitting parameters are the diffusion coefficients D_f and D_s, the $h_\mathrm{df} = R_\mathrm{f}d/D_\mathrm{f}$, $h_\mathrm{ds} = R_\mathrm{s}d/D_\mathrm{s}$, $\Delta A_{\mathrm{f}\infty}$ and $\Delta A_{\mathrm{s}\infty}$.

The fitting procedure uses the Levenberg–Marquardt method [24]. The fitting accuracy is estimated by the reduced χ^2 criterion [24]:

$$\chi^2 = \frac{1}{N_\mathrm{p} - N_\mathrm{var}}\sum_{i=1}^{n}(\Delta A(t_i) - \Delta A_i^{\mathrm{exp}})^2, \tag{8}$$

where N_p is the number of experimental points for which the fitting is carried out, N_var is the number of fitting parameters, $\Delta A(t)$ is the fitting function and $\Delta A_i^{\mathrm{exp}}$ is the experimental value of the absorbance change at time t_i. The standard error of the fitting parameters is estimated as

$$\sigma_j = \sqrt{C_{jj}\chi^2}, \tag{9}$$

where j is the number of the fitting parameter, $j = 1, \ldots 6$, C_{jj} is the diagonal element of the variance–covariance matrix determined as $C = (J_T \cdot J)^{-1}$, J represents the Jacobian, i.e. the matrix with the elements $\partial(\Delta A(t_i))/\mathrm{d}x_j$, x_j are the fitting parameters [24].

The results of the approximation are shown in figure 4. As is seen from the graphs, the diffusion model allows us

Table 2. The fitting accuracies χ^2 of the approximations.

Temperature (K)	688	773	863	928	1013
			Oxidation		
Two diffusion processes	3.4×10^{-8}	3.9×10^{-7}	6.4×10^{-7}	2.3×10^{-6}	5.7×10^{-6}
Diffusion + reaction	1.7×10^{-7}	1.8×10^{-7}	1.8×10^{-7}	7.4×10^{-6}	1.7×10^{-6}
			Reduction		
Two diffusion processes	1.5×10^{-7}	3.8×10^{-6}	5.6×10^{-6}	7.5×10^{-7}	3.6×10^{-7}
Diffusion + reaction	4.9×10^{-7}	1.0×10^{-6}	2.2×10^{-6}	3.5×10^{-6}	2.2×10^{-6}

to obtain a good approximation of the experimental kinetic curves. The values of the χ^2 criterion are found to range between $\sim 1.5 \times 10^{-7}$ and $\sim 5.5 \times 10^{-6}$. However, in most cases the standard errors, equation (9), are small only for the values of the maximum absorbance changes $\Delta A_{f\infty}$ and $\Delta A_{s\infty}$. The diffusion coefficients are correctly determined only for some experimental kinetics. In particular, from the fitting of the kinetics of oxidation at 688 K we obtain values of $D_f = (6.30 \pm 0.11) \times 10^{-7}$ cm^2 s^{-1} and $h_{df} = 1.004 \pm 0.003$ which correspond to a mass-transfer coefficient of $R_f = (7.03 \pm 0.13) \times 10^{-6}$ cm s^{-1}. The diffusion coefficient D_f obtained from the kinetics of the reduction at the same temperature amounts to $(7.33 \pm 0.15) \times 10^{-7}$ cm^2 s^{-1}, i.e. it is sufficiently close to the one obtained for oxidation. It must be mentioned that the contribution of the slow diffusion process turns out to be insignificant at 688 K and may not be taken into consideration. The value of h_{df} for reduction at 688 K is 0.421 ± 0.014 which corresponds to a mass-transfer coefficient of $R_f = (3.43 \pm 0.13) \times 10^{-6}$ cm s^{-1}. Thus, the density of the oxygen flow from the surroundings to the crystal surface during oxidation at 688 K is approximately twice as large as the density of the backward flow during reduction. In addition, at 1013 K we obtain an estimate of $D = (2.2 \pm 0.6) \times 10^{-6}$ cm^2 s^{-1} for one of the diffusion coefficients in reduction; due to the large error margins of the second diffusion coefficient, the terms 'fast' and 'slow' cannot be assigned here.

4.2. Model 'diffusion + reaction'

In this model, we proceed from the assumption that the absorption centres in $YbAlO_3$ can be identified as $(O_O^- Yb_{Al}^{3+})^\bullet$. Thus, the decrease of the absorbance in the spectral range of 300–600 nm during reduction can be considered as being due to the following quasi-chemical reaction:

$$2(O_O^- Yb_{Al}^{3+})^\bullet + V_O^x \longrightarrow 2O_O^x + (Yb_{Al}^{3+} V_O^0 Yb_{Al}^{3+})^{\bullet\bullet}. \quad (10)$$

The associates $(Yb_{Al}^{3+} V_O^0 Yb_{Al}^{3+})^{\bullet\bullet}$, formed according to equation (10), are considered as non-absorptive in the spectral range 200–600 nm. The oxygen vacancies V_O^x that participate in the reaction (10) are formed due to the excorporation of the oxygen from the crystal during reduction according to

$$O_O^x \rightarrow 0.5O_2(g) + V_O^x. \quad (11)$$

The processes, taking place during oxidation, are inverse ones to the ones described by equations (10)–(11).

Let the forward process in (10) be characterized by the rate constant k_f and the backward process by the rate constant k_b. Taking into account the diffusion of oxygen vacancies, a mathematical model describing the kinetics in the defect subsystem of the crystal can be represented by the following system of differential equations:

$$\begin{aligned} \frac{\partial n_V}{\partial t} &= D\frac{\partial^2 n_V}{\partial^2 x} - k_f n_a^2 n_V + k_b n_y, \\ \frac{1}{2}\frac{\partial n_a}{\partial t} &= -k_f n_a^2 n_V + k_b n_y, \\ \frac{\partial n_y}{\partial t} &= k_f n_a^2 n_V - k_b n_y. \end{aligned} \quad (12)$$

Here, D is the oxygen vacancy diffusion coefficient, n_V is the concentration of the vacancies, n_a is the concentration of the absorption centres $(O_O^- Yb_{Al}^{3+})^\bullet$ and n_y is the concentration of the associates $(Yb_{Al}^{3+} V_O^0 Yb_{Al}^{3+})^{\bullet\bullet}$. The initial conditions for the system (12) are: $n_V(t = 0, x) = N_{V0}$, $n_a(t = 0, x) = N_{a0}$, $n_y(t = 0, x) = N_{y0}$. The boundary conditions for (12) are, as before, third-order ones (4). After solving for system (12), the changes of the absorbance during annealing $\Delta A(t)$ were calculated according to equation (5).

The fitting procedure for the 'diffusion + reaction' model is based on a numerical solution of the system (12) by the finite difference method, thereby normalizing all concentrations to the initial concentration of associates, N_{y0}. Taking into account the relationship between the initial reagent concentrations

$$k_f N_{a0}^2 N_{V0} = k_b N_{y0}, \quad (13)$$

the number of fitting parameters can be decreased to seven: D_V, R, N_{V0}, N_{Vf}, k_f, k_b and the coefficient k_a which is proportional to the cross section σ of the absorption centres. As before, the Levenberg–Marquardt method was used for fitting. The fitting accuracy was estimated by the criterion (8) and the precision of the fitting parameters by criterion (9).

As it follows from our calculations, model (12) allows us to obtain a quality of fit which is comparable to the one reached by the diffusion model (6) (table 2). The calculated theoretical kinetics is also close to the ones of the diffusion model shown in figure 4. Generally, the 'diffusion + reaction' model is slightly better in describing the experimental kinetics of oxidation. The theoretical dependences obtained in the framework of this model are practically indistinguishable from the ones shown in figure 4. The precision of the determination of the fitting parameters is unsatisfactory. Obviously, this

is caused by a superposition of the errors of the numerical methods used for the solution of system (12), for the determination of the absorbance changes (5) and for the calculation of the derivatives $\partial(\Delta A(t_i))/\mathrm{d}x_j$ required by the optimization procedure. Nevertheless, the obvious advantage of this model in comparison with the diffusion model is the absence of the assumption about a second diffusion mechanism, the physical nature of which is uncertain.

5. Conclusions

Ytterbium orthoaluminate possesses the orthorhombic $GdFeO_3$ type of structure in a wide temperature range of 4–1173 K. Similar to other $RAlO_3$ perovskites, thermal expansion of ytterbium orthoaluminate displays strongly anisotropic and nonlinear behaviour. However, in contrast to the majority of $RAlO_3$ compounds possessing the orthorhombic structure, there are no visible anomalies in the thermal expansion of $YbAlO_3$ in the temperature range of 19–1173 K.

The high-temperature oxidizing annealing leads to an increase of optical absorption in the spectral range from 300 to 600 nm. The high-temperature annealing of $YbAlO_3$ crystal in a reducing atmosphere results in the disappearance of this absorption band. The processes of formation and disappearance of the absorption band are reversible; their durations become shorter with increasing temperatures and remain comparable at each temperature.

High-temperature redox annealing of the $YbAlO_3$ crystal at temperatures up to 1013 K does not lead to recharging of ytterbium, contrary to the case of $Yb_3Al_5O_{12}$ crystals and $Yb{:}Y_3Al_5O_{12}$ epitaxial films where $Yb^{3+} \leftrightarrow Yb^{2+}$ recharging was observed.

Experimental kinetics of the absorbance changes during oxidation and reduction can successfully be described by two different models. The first of them assumes the presence of two diffusion mechanisms—a fast and a slow, in which two species of defects can be associated with oxygen vacancies and, possibly, with cation vacancies. The second model does not need the assumption about two diffusion processes. It takes into consideration not only diffusion but also the kinetics of redox processes of the defects. The accuracy of fitting for both models is sufficiently high ($\chi^2 \sim 10^{-7}$–10^{-5}) and comparable. However, the precision of determination of the individual fitting parameters is unsatisfactory for the majority of the experimental kinetics. Only for kinetics registered at 688 K, the first model allows us to obtain reliable values for the diffusion and mass-transfer coefficients of the fast diffusion process $D_\mathrm{f} = (6.30 \pm 0.11) \times 10^{-7}$ cm^2 s^{-1}, $R_\mathrm{f} = (7.03 \pm 0.13) \times 10^{-6}$ cm s^{-1} (i.e. $h_{df} = 1.004 \pm 0.003$) for oxidation and $D_\mathrm{f} = (7.33 \pm 0.15) \times 10^{-7}$ cm^2 s^{-1}, $R_\mathrm{f} = (3.43 \pm 0.13) \times 10^{-6}$ cm s^{-1} (i.e. $h_{df} = 0.421 \pm 0.014$) for reduction. In addition, for reduction at 1013 K we estimate one of the diffusion coefficients of $D = (2.2 \pm 0.6) \times 10^{-6}$ cm^2 s^{-1}.

Acknowledgments

The work was partially supported by the Ukrainian Ministry of Education and Science (project no. 0109U001160, Acronym: Tern and no. 0108U004774, Acronym: M/53-2008) and by the German Ministry of Education and Research (WTZ Project UKR 06/003). The support by G B Loutts from Norfolk State University (VA, USA) in providing the $YbAlO_3$ crystals is gratefully acknowledged. LV thanks H Schmidt, C Paulmann, M Knapp and C Bähtz for their kind assistance during x-ray single-crystal and *in situ* low- and high-temperature powder diffraction experiments at HASYLAB.

References

[1] Chipaux R, Cribier M, Dujardin C, Garnier N, Guerassimova N, Mallet J, Meyer J-P, Pédrini C and Petrosyan A G 2002 *Nucl. Instrum. Methods* A **486** 228–33
[2] Wong H T-K and Li J 2001 *Proc. Ist NCTS Workshop (Kenting, Dec. 2001)* pp 65–76
[3] Noginov M A, Loutts G B, Ross K, Grandy T, Noginova N, Lucas B D and Mapp T 2001 *J. Opt. Soc. Am.* B **18** 931–41
[4] Blessing R H 1995 *Acta Crystallogr.* A **51** 33–8
[5] Knapp M, Baehtz C, Ehrenberg H and Fuess H 2004 *J. Synchrotron. Radiat.* **11** 328–34
[6] Knapp M, Joco V, Baehtz C, Brecht H, Berghaeuser A, Ehrenberg H, von Seggern H and Fuess H 2004 *Nucl. Instrum. Methods* A **521** 565–70
[7] Ihringer J and Küster A 1993 *J. Appl. Crystallogr.* **26** 135–7
[8] Akselrud L G, Zavalij P Yu, Grin Yu, Pecharsky V K, Baumgartner B and Woelfel E 1993 *Mater. Sci. Forum* **133–136** 335
[9] Vasylechko L, Savytskii D, Schmidt H, Bismayer U, Matkovskii A, Loutts G and Paulmann C 2000 *HASYLAB Annual Reports* vol 1 p 599
[10] Vasylechko L, Matkovskii A, Senyshyn A, Savytskii D, Knapp M and Bähtz C 2003 *HASYLAB Annual Reports* vol 1 p 251
[11] Vasylechko L, Senyshyn A and Trots D M 2007 *HASYLAB Annual Reports* vol 1 pp 469–70
[12] Sugak D, Zhydachevskii Ya, Sugak Yu, Buryy O, Ubizskii S, Solskii I, Schrader M and Becker K D 2007 *J. Phys.: Condens. Matter* **19** 086211
[13] Sugak D, Zhydachevskii Ya, Buryy O, Ubizskii S, Börger A, Schrader M and Becker K D 2008 *Acta Mater.* **56** 6310–8
[14] Sugak D, Zhydachevskii Ya, Sugak Yu, Buryy O, Ubizskii S, Solskii I, Börger A and Becker K D 2009 *Phys. Chem. Chem. Phys.* **11** 3138–43
[15] Radhakrishna P, Hamman J, Ocio M, Pari P and Allain J 1981 *Solid State Commun.* **37** 813
[16] Vasylechko L, Senyshyn A and Bismayer U 2009 Perovskite-Type Aluminates and Gallates *Handbook on the Physics and Chemistry of Rare Earths* vol 39 ed K A Gschneidner Jr, J-C G Bünzli and V K Pecharsky (Netherlands: North-Holland) pp 113–295
[17] Zeng X, Zhao G, Xu X, Li H, Xu J, Zhao Z, He X, Pang H, Jie M Y and Yan C 2005 *J. Cryst. Growth* **274** 106–12
[18] Shim J B, Yoshikawa A, Fukuda T, Pejchal J, Nikl M, Sarukura N and Yoon D H 2004 *J. Appl. Phys.* **95** 3063–7
[19] Kreye M and Becker K D 2003 *Phys. Chem. Chem. Phys.* **5** 2283–90
[20] Martynyuk N V, Ubizskii S B, Buryy O A, Becker K D and Kreye M 2005 *Physica Status Solidi* c **2** 330–3
[21] van Pieterson L, Heeroma M, de Heer E and Meijerink A 2000 *J. Lumin.* **91** 177
[22] Saiful Islam M 2002 *Solid State Ion.* **154/155** 75–85
[23] Crank J 1955 *The Mathematics of Diffusion* (Oxford: Clarendon)
[24] Press W H, Flannery B P, Teukolsky S A and Vetterling W T 1989 *Numerical Recipes in Pascal. The Art of Scientific Computing* (Cambridge: Cambridge University Press)